Chapter

Spatial Light Modulation as a Flexible Platform for Optical Systems

Cátia Pinho, Isiaka Alimi, Mário Lima, Paulo Monteiro and António Teixeira

Abstract

Spatial light modulation is a technology with a demonstrated wide range of applications, especially in optical systems. Among the various spatial light modulator (SLM) technologies, e.g., liquid crystal (LC), magneto-optic, deformable mirror, multiple quantum well, and acoustic-optic Bragg cells, the ones based on liquid crystal on silicon (LCoS) have been gaining importance and relevance in a plethora of optical contexts, namely, in telecom, metrology, optical storage, and microdisplays. Their implementation in telecom has enabled the development of high-capacity optical components in system functionalities as multiplexing/demultiplexing, switching and optical signal processing. This technology combines the unique light-modulating properties of LC with the high-performance silicon complementary metal oxide semiconductor properties. Different types of modulation, i.e., phase, amplitude or combination of the two, can be achieved. In this book chapter, we address the most relevant applications of phase-only LCoS SLM for optical telecom purposes and the employment of SLM technology in photonic integrated circuits (PICs) (e.g., field-programmable silicon photonic (SiP) circuits and integrated SLM application to create versatile reconfigurable elements). Furthermore, a new SLM-based flexible coupling platform with applications in spatial division multiplexing (SDM) systems (e.g., to efficiently excite different cores in MCF) and characterization/testing of photonic integrated processors will be described.

Keywords: spatial light modulator (SLM), liquid crystal silicon (LCoS) SLM, optical transforms, computer-generated holography (CGH), photonic integrated circuits (PICs), spatial division multiplexing (SDM)

1. Introduction

There has been significant growth in the required capacity of the telecommunication systems, which can be attributed to the proliferation of mobile devices, bandwidth-intensive applications, and services [1–3]. As a result, a significant increase in the broadband connections as well as the related multimedia traffic on a yearly basis [4–6] has been progressing. Moreover, the traffic explosion has been one of the challenges being faced in telecommunication systems [2, 7]. Also, it has been observed that the traditional electronic media which are based on copper are unable to meet the system requirements majorly in terms of bandwidth and latency [5, 8–10].

To address the challenges, optical fiber-based transport systems have been employed in different fields of communication systems as viable and reliable solutions. The widely employed optical transport systems are based on single-mode fiber (SMF). To enhance the capacity of single-core SMF, advanced modulation formats and wavelength division multiplexing (WDM) are normally employed. However, the growing demand for further video/image storage capacity and the increase in cloud service adoption, which is as a result of numerous smartphones and other Internet-based gadgets, have led to research on solutions for effective bandwidth optimization [11, 12]. This is due to the fact that the conventional SMF-based transport systems have been observed to be approaching Shannon's limit [13] and the achievable maximum capacity will not be sufficient to support the envisaged massive connection demanded by the next-generation networks [5, 14–16]. Besides the capacity that is expected to be saturated around 100 Tbit/s owing to the physical limits, the conventional SMF schemes with WDM might be unable to meet the power consumption, spatial efficiency, and cost requirements of the communication systems [16, 17].

There has been considerable attention on multicore fiber (MCF) as a feasible solution capable of addressing the capacity limit of a conventional SMF-based scheme [15, 18, 19]. For effective implementation of MCF, the research community has been working diligently on improved cost-efficient and scalable networking infrastructure solutions. A notable optical transport scheme that can exploit the space dimension in order to address the optical system capacity crunch and improve the system performance is spatial division multiplexing (SDM) [19]. Moreover, it has been observed that MCF is an efficient and main enabling technology for the SDM systems [16, 18]. Apart from the MCF, SDM implementation for multimode fiber (MMF) has also been attracting significant attention [17, 18]. Nevertheless, the MCF implementation is susceptible to and can be constrained by the transmission impairments such as nonlinearities and inter-core cross talk (XT) between signals at the neighboring cores that may be presented via multiple optical paths. This may have a significant effect on the system performance regarding the transmission range and the network size [16, 17]. Furthermore, the extent of the presented performance degradation by the transmission impairments varies with the MCF fiber types (i.e., 3-core, 7-core, 13-core, 19-core, 37-core, and 61-core) [16, 20]. A practical solution for addressing the MCF implementation challenges is spatial light modulation.

Spatial light modulators (SLM) can be employed for exciting different cores and/or modes in order to mitigate the transmission impairments introduced by multiple optical paths, as it enables arbitrary removal or addition of channels with the aid of software, i.e., implementation of a diffractive optical element by computer-generated holograms (CGH). Due to the SLM support for dynamic reconfiguration of optical wave fronts, it can be employed for core and mode multiplexing and demultiplexing [5, 21, 22]. In addition, the use of silicon photonic (SiP) onboard transceivers that are coupled on the MCF for supporting transmissions has been shown to be promising. This is due to the fact that there is no need for fan-in/fan-out or core pitch conversion devices that may give rise to further system complexity [16].

Optical communication evolution has brought about the emergence of improved photonic integrated circuits (PICs) that present economic and sustainable alternative to data transmission [9]. Therefore, it is expected to be an enabling technology, capable of contributing significantly in a number of fields [8]. As a result, various benefits are offered, such as small weight and volume, low power consumption, high mechanical and thermal stability, and the ease of assembling a number of complex systems.

PIC can be generally characterized as a multiport device with an integrated system of optical elements such as attenuators, modulators, multiplexers, detectors, lasers, and optical amplifiers that are embedded in a single chip using a waveguide (WG) architecture [23]. However, it has been observed that optical component testing is very challenging and time-consuming as well [24]. This can be attributed to the required tight three-dimensional (3D) alignment tolerances, to ensure accurate light coupling. Hence, with notable development and growing adoption of PIC in the communication networks, advanced methods are imperative for an accurate PIC performance testing as well as characterization. As aforementioned, based on the support for dynamic reconfiguration of light, SLM can be employed for optical PIC testing and characterization, by exploring this feature in the feeding and/or receiving the optical signal into the PIC [8, 23].

In this chapter, we focus on the most pertinent applications of phase-only liquid crystal on silicon (LCoS) SLM for optical telecom purposes and the employment of SLM technology in PIC, e.g., field-programmable silicon photonic circuits and integrated SLM application to create versatile reconfigurable elements. Furthermore, a new SLM-based flexible coupling platform for applications in SDM systems and characterization/testing of photonic processors will be presented.

In Section 2, SLM working principle and their applications in telecom are addressed in more detail. The applied methodology (i.e., algorithms and experimental setup) to create a diffraction optical element through the implementation and optimization of CGH is described in Section 3. In Section 4, discussion on the obtained results from the experimental implementation of CGH for SDM and PIC applications is presented. An overall conclusion regarding the employment of the SLM technology as a flexible platform for optical systems is provided in Section 5.

2. Spatial light modulator (SLM)

Optical signal processing has been providing relevant solutions to convert data into spatially modulated coherent optical signals with SLM devices, allowing the effective implementation of digital holograms [25]. One of the most useful properties of the hologram is its ability to control phase and amplitude of light in the far field. The Fourier transform describes the relationship between a hologram (near field) and its corresponding replay field (far field). The far field can be formed at the focal point of a positive lens or an infinite distance from the near field plane in free space [25, 26], as depicted in **Figure 1**.

Holograms can reproduce waveforms from an existing object. With digital advances and optical signal processing, it is possible to numerically calculate interference patterns to generate completely synthetic wave fronts of arbitrary form. These interference patterns can have different denominations, such as CGH, diffractive optical elements (DOE), phase/amplitude masks, diffractive grating, etc. [26]. All operate in the principle of diffraction, so it is somehow an arbitrary choice of terminology.

The SLM is a device that can be used to modulate light in accordance with a fixed spatial (pixel) pattern and can be programed electrically. Usually, it can be exploited for incident light phase and/or amplitude control. Subsequently, phase-only, amplitude-only, or the combination of phase-amplitude can be readily realized with SLM. There are a number of modulation mechanisms that can be employed. One of the attractive and widely used ones is electro-optical SLM. The

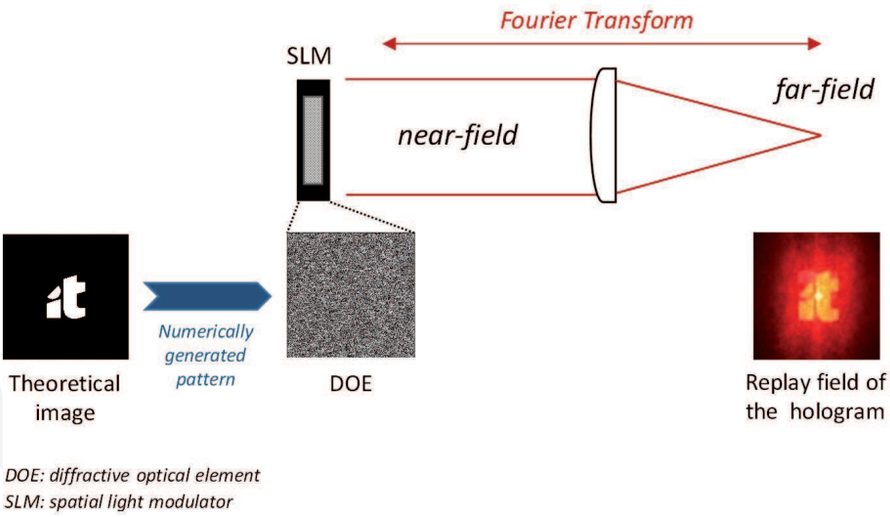

Figure 1.
Diagram of a Fourier transform through a positive lens. A complex design pattern (diffractive optical element (DOE)) is provided to the SLM to generate the expected hologram in the replay field (far field).

modulation material of electro-optical SLM is liquid crystal. Similarly, a liquid crystal SLM has a microdisplay being employed for the incident light modulation and collection. This can be realized in a transmissive form using a liquid crystal display (LCD) SLM technology or in a reflective form with LCoS SLM technology. One of the leading features of the modulators is in the liquid crystal molecule alignment. Typically, this can be either vertical, parallel, or with twisted formation. Consequently, with suitable polarizing optics, this influences the incident light beam properties that can be effectively changed, i.e., amplitude, phase, or their combination [8, 23, 27].

It should be noted that the common hologram generation techniques cannot arbitrarily modulate the beam phase and amplitude concurrently [26, 27]. Therefore, it is unrealistic to basically address the desired pattern inverse Fourier transform into the far field and replicate the resulting amplitude and phase distribution directly on the SLM. As a consequence, the employment of optimization algorithms is highly recommended for evaluating the best potential hologram within the device constraints, e.g., the best pixel distribution in which each pixel will be able to take only one of two states that correspond to a 0 or π phase shift [23, 26].

The nematic LCoS technology is a type of SLM with phase-only modulation capability. Moreover, it is an electrically addressed reflection modulator category in which a direct and accurate voltage controls the liquid crystal and the light beam wave front can be modulated as well [28, 29]. An example of an LCoS SLM is illustrated in **Figure 2** [23]. The LCoS SLM can be employed as a diffractive device for reconstructing images from CGH [30].

CGH can be employed for different communication purposes and has been gaining application in indoor visible light communication systems [31]. Furthermore, suitable holograms can be readily generated by employing a variety of optimization techniques such as iterative Fourier transform algorithm (IFTA) [5, 32–34]; linear Fourier transform (i.e., linear phase mask) [5, 18, 23, 35]; simulated annealing [36]; and Gerchberg-Saxton algorithm [37]. The employment of the SLM as a diffractive device for reconstructing images from CGH permits the light beam wave front to be modulated [8, 23].

As aforementioned, LCoS displays have been gaining significant recognition as promising microdisplays for various types of SLM applications. Similarly, they possess attractive and significant features like very high spatial resolution and

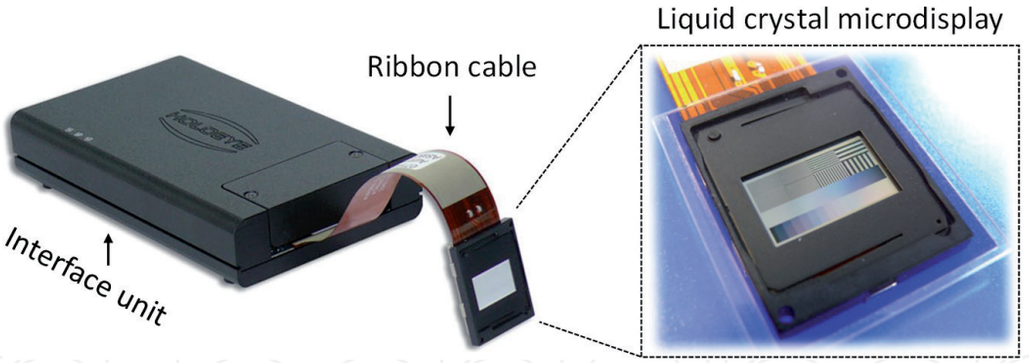

Figure 2.
LCoS SLM Pluto phase modulator from Holoeye© 2018 Holoeye photonics AG.

light efficiency [38]. Due to this, they have been applicable in a plethora of optical contexts such as communication, reconfigurable interconnects [39], storage [40], diffractive optics [41], metrology [42], and quantum computing [43]. They are also applicable in the wave shaper technology for optical signal processing and monitoring [44]. In addition, other advantages of the LCoS are that it is highly cost-effective and can as well be flexibly programmed. This helps in supporting a number of additional functions like group delay ripple compensation, wavelength filtering, and chromatic dispersion compensation. Besides, it can aid in ensuring variable attenuation for individual wavelength channels as well as output ports. Consequently, LCoS device offers a cost-effective and promising solution for the wavelength selective switch (WSS) [40].

The LCoS microdisplay SLM has a good implementation history in the WSS systems. Its employment in the WSS system core component can be attributed to a number of advantages such as larger spatial bandwidth, more port availability, and enhanced resolution, as well as the system miniaturization. The WSS systems have been exploited in the reconfigurable optical add/drop multiplexers (ROADM) in WDM optical networks. It has been observed that ROADM is one of promising schemes that can be employed to improve on the traffic capacity of the existing and future telecommunication systems [40, 45]. Moreover, in communication networks, the ease of adding or dropping the wavelength is essential. They can ensure effective information access or rerouting to another appropriate path in the network. It should be noted that WSS is the ROADM sub-system that has been extensively employed in optical switch applications. In addition, microelectromechanical systems (MEMS) [46] and WSS based on LCoS [47] have been commercialized for different applications. Also, WSS by means of LCoS operates on the principle of "disperse and select," in which the inward bound WDM channels are dispersed into a distinct wavelength channel and subsequently relayed by LCoS through programmable grating patterns. This is in an attempt to facilitate an add and drop function. It is envisaged that the next-generation ROADM will hold different attractive features such as directionless, colorless, and contentionless in order to improve the system performance [40].

Furthermore, LCoS technology can also be employed in flex grid that has been considered as the major feature for the next-generation networks [40, 48]. It should be noted that the traditional fixed grid with 50 GHz spacing standardized by the International Telecommunication Union (ITU) Telecommunication Standardization Sector (ITU-T) possesses a number of challenges. The fixed grid has been observed to bring about the optical spectra being inefficiently used. Besides, it constrains the system transmission capacity considerably. On the other hand, the flex grid implementation enables the use of different modulation formats

and their coexistence on a shared infrastructure. They can also be densely and efficiently multiplexed which aids the optical networks, not only to extend the reach but also the per channel bit rate. It has also been envisaged that implementation of WSS and SDM will significantly help further in extending the network reach and capacity [40].

3. Methodology

The adopted methodology to implement the SLM flexible platform for optical systems can be subdivided into two main sections: (i) the algorithms employed for the CGH generation and optimization methodology (in Section 3.1) and (ii) the SLM framework setup implementation with application in SDM systems and characterization/testing of PIC (in Section 3.2).

The framework ability to improve the overall alignment process and excite different cores of a MCF, can provide a valuable contribution for the impairment mitigation of the system optical path, which can relax digital signal processing (DSP) equalization requirements of the SDM system [5, 18, 22, 34, 49].

Furthermore, its use as a flexible platform for feeding photonic integrated processors was also explored for the characterization/test of PICs, and results have been presented for its implementation as a parallel implementation of the Haar transform (HT) image compression algorithm [8, 18, 23].

3.1 CGH pattern establishment

Holography is a 3D-based display system that comprises exploiting diffraction and interference for recording and reconstructing optical wave fronts. Moreover, computer-generated holography is an effective technique that is appropriate for a broad variety of displays such as two-dimensional (2D), volumetric, autostereoscopic, stereoscopic, and true 3D imaging. It is remarkable that the CGH is becoming feasible due to the emergence of progressively powerful computers that prevents the conventional interferometric recording step in the formation of hologram [50]. In addition, the CGH can be viewed as a phase mask with spatially variable transmittance or a diffractive optical element that can be readily displayed on the devices such as SLM, which are capable of diffracting light [5, 51]. Also, the information that needs to be transformed is presented to an optical system, through the SLM. This is effected with a suitable phase mask for the concerned input function [25].

From a set of different available techniques for the generation of CGH (e.g., IFTA, linear Fourier transform, simulated annealing, and Gerchberg algorithm, as described in Section 2), in our SLM framework, higher focus was given to the linear Fourier transform principle for the calculus of the numerical interference patterns to generate the holograms (CGH). This decision was mainly due to the intensive computational requests and high power loss (up to 9 dB [26]) associated with the implementation of the simulated annealing and Gerchberg-Saxton algorithms and additional computational cost of IFTA when compared to linear phase mask.

Thus, a simplified approach based on the implementation of a linear phase mask generation (in Section 3.1.1) and the development of a new iterative algorithm experimentally driven for CGH effective optimization (in Section 3.1.2) is proposed and tested.

All algorithms were developed and implemented in MATLAB© [52].

3.1.1 Linear phase mask CGH

A linear phase mask can be described as a numerical information transformation (in the Fourier domain) of the input function of interest [25], which can be introduced into the optical system through an SLM.

The CGH implemented with a linear phase mask can be expressed in the frequency domain as expressed in Eq. (1) [5, 23], where f_x and f_y denote the spatial frequency vector components that correspond to the image to be generated in both X and Y axes, respectively, and c_x and c_y represent the horizontal and vertical tilt parameters, respectively.

$$M_{linear} = M(f_x, f_y) = -2\pi(c_x f_x + c_y f_y) \tag{1}$$

A collimated Gaussian beam with transverse profile S_{in} is imaged onto the SLM via a lens, Eq. (2), where (x_0, y_0) offer the horizontal and vertical position, respectively, and (w_x, w_y) represent the width and the height of the beam, respectively, as depicted in **Figure 3** [8].

$$S_{in} = exp\left(-\left(2\frac{x - x_0}{w_x \log(\sqrt{2})}\right)^2 - \left(2\frac{y - y_0}{w_y \log(\sqrt{2})}\right)^2\right) \tag{2}$$

With the adoption of Fraunhofer approximation, the Fourier transform is produced on the SLM plane, $fft(S_{in})$. Afterward, the subsequent illumination profile is multiplied with the phase mask, $e^{iH_{mask}}$. The resultant signal is then Fourier transformed via the second lens by means of an inverse Fourier transform to achieve the output signal S_{out}, which can be defined as Eq. (3) [5, 8]:

$$S_{out} = ifft(H(fft(S_{in}))) \tag{3}$$

A graphical user interface (GUI) was also developed to test different masks to be applied to the SLM device [18] (see **Figure 4**).

Different phase masks can be attained by adjusting the different available parameters from the developed GUI. For the *Input Beam* GUI panel the following

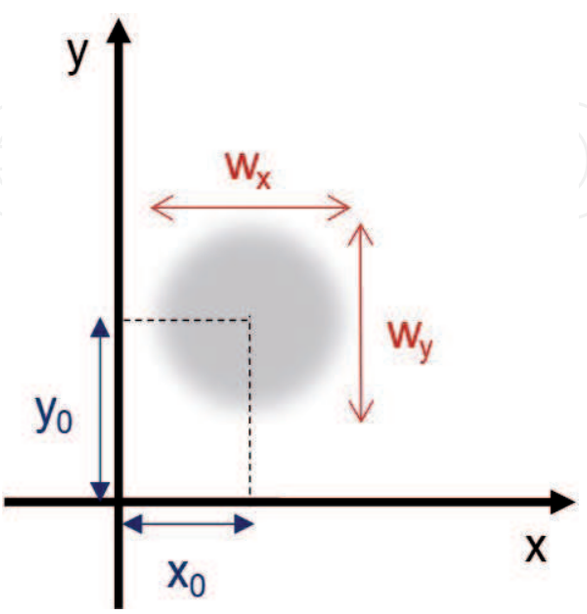

Figure 3.
Cartesian coordinate system description of the parameters (x_o, y_o) and (w_x, w_y) employed for the input beam S_{in} estimation [8].

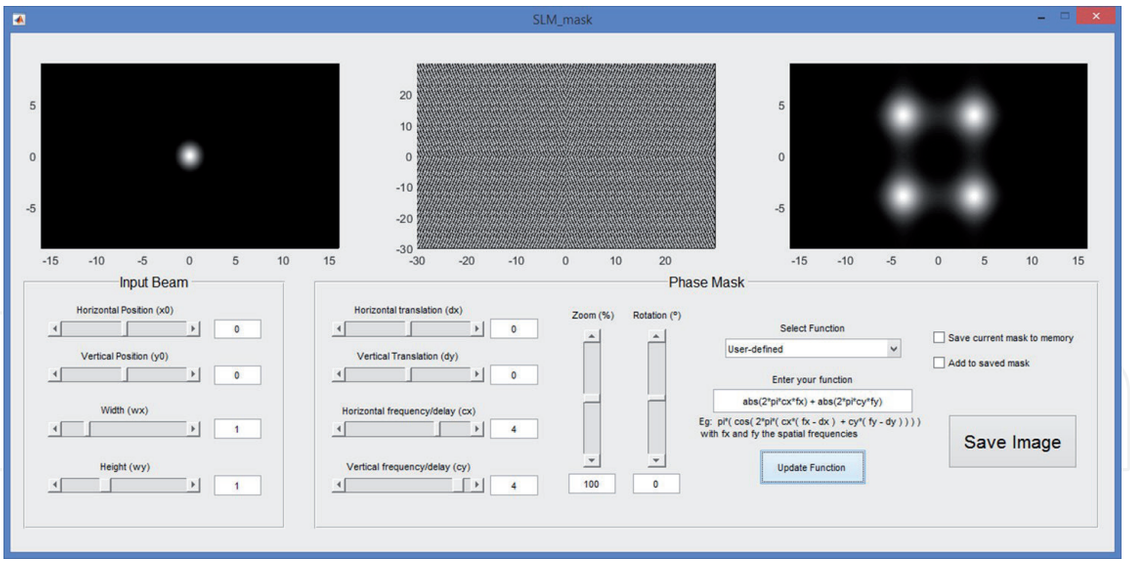

Figure 4.
GUI SLM_mask to generate the different phase masks applied to the SLM [18].

input parameters are available: (i) horizontal position (x_0); (ii) vertical position (y_0); (iii) width of the beam (w_x); and (iv) height of the beam (w_y) (see GUI panel *Input Beam* in the **Figure 4**).

$$S_{out} = ifft\left(H\left(fft\left(S_{in}\right)\right)\right) \tag{4}$$

The Phase Mask GUI panel offers the correspondent input parameters: (i) horizontal translation (d_x); (ii) vertical translation (d_y); (iii) horizontal frequency delay (c_x); (iv) vertical frequency delay (c_y); (v) percentage of zoom (%); (vi) rotation in degrees (°); and (vii) selection of three possible input functions, i.e., sinusoidal Eq. (4), linear Eq. (1), or defined by the user (user-defined). The option to save or replace the phase mask file is also made available, as depicted in the Phase Mask GUI panel from **Figure 4**.

The implemented scripts and GUI were written in MATLAB© [52].

3.1.2 Optimization of the linear phase mask CGH

In an effort to realize the hologram that can suitably replicate the output signal, we estimated the hologram of the beam through the image phase-only information of the generated hologram. Thus, a first linear phase mask is generated to produce the expected initial field, i.e., the input function of interest.

Since a phase-only SLM does not permit the inverse Fourier of the desired pattern to be addressed into the far field and replicated into the resultant distribution of amplitude and phase on the SLM directly. It is quite demanding to generate a CGH with guarantees for the light to be spatially modulated with the required accuracy and resolution. To address these challenges and obtain the desired hologram with an error factor $\delta \leq 10\%$, we implemented an iterative algorithm to optimize the generation of the linear phase mask. Also, the error factor threshold was set so as to prevent an infinite loop in the adopted optimization algorithm, while guaranteeing that the output result has an accuracy $\geq 90\%$.

The algorithm was implemented to generate a hologram that replicates the output of the four waveguides (WG) of an optical chip for data compression proposes [8, 23, 53]. A hologram of four beams was calculated by a phase-only

superimposition of four independent holograms generated by Eq. (1). Then, the corresponding linear transformations in the Fourier domain provided in Eq. (5) and Eq. (6) were applied [8, 23]:

$$H = \angle\left(e^{iH_1} + e^{iH_2} + e^{iH_3} + e^{iH_4}\right) \tag{5}$$

$$H_1 = exp\left(i2\pi\left(c_{x1}f_x + c_{y1}f_y\right)\right) \tag{6}$$

The block diagram of the employed algorithm is given in **Figure 5**, and the major steps of the algorithm are enumerated as follows [23]:

i. Generate a first linear phase mask to produce the expected initial field based on Eq. (5).

ii. Initially set the four values $a_{1\text{-}4}$ to 1, from $H = \angle\left(a_1 e^{iH_1} + a_2 e^{iH_2} + a_3 e^{iH_3} + a_4 e^{iH_4}\right)$.

iii. Acquire the replay field from the hologram generated by SLM (*I SLM*) with a camera, and feed this data to the algorithm.

iv. Calculate the difference between the hologram generated and the initial field expected, defined as error factor: $\delta = |I_{SLM} - I_1| \leq 0.1$.

v. If the condition $\delta \leq 0.1$ is not satisfied, repeat steps ii–iv by iteratively adjusting the values of $a_{1\text{-}4}$ to compensate for the error factor.

The developed algorithm in MATLAB® is capable of controlling both SLM and camera hardware, providing a dynamic experimentally driven algorithm for effective CGH optimization.

The error factor (δ) is defined to quantify the generated hologram deviation from the optical chip anticipated output [8, 23].

3.2 CGH generation setup

The employed SLM is a reflective LCoS phase-only type, and its model is PLUTO-TELCO-012. It can operate within the wavelength range of

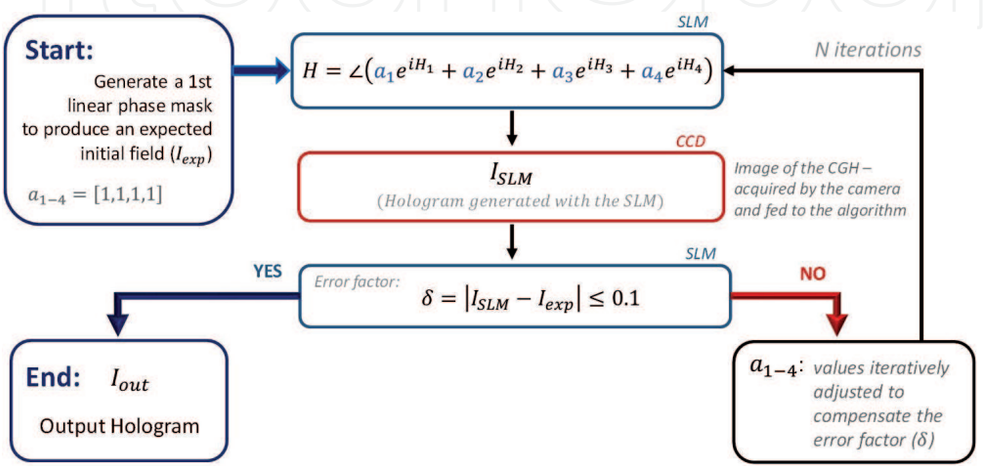

Figure 5.
Block diagram of the algorithm applied for the optimization of the linear phase mask CGH [23].

1400–1700 nm. Additionally, an active area of 15.36 × 8.64 mm^2, a pixel pitch of 8.0 μm, a 92% fill factor, and 80% reflectivity are employed for displaying the generated hologram.

Two different setup arrangements were implemented to create CGH for SDM (e.g., MCF) and PIC applications.

3.2.1 CGH setup for SDM

Setup alignments were carried out, using a red laser of 637 nm (power 70 mW, SM fiber-pigtailed laser diode), a collimator, two lenses, a charge-coupled device (CCD) image sensor, and the LCoS-SLM. After the alignments, an MCF of 10 m of length and a bit error rate (BER) tester were introduced in the setup, as depicted in **Figure 6**.

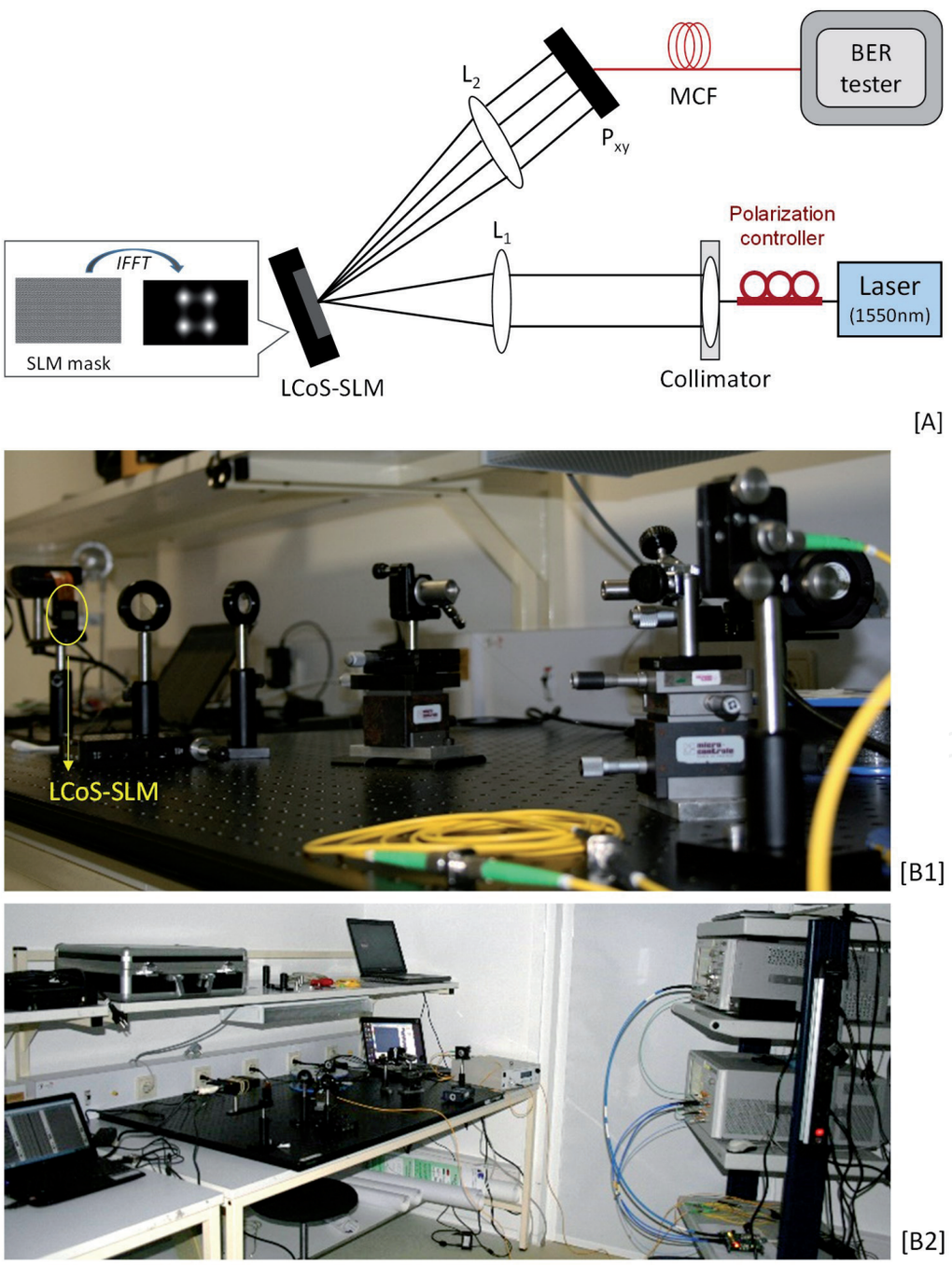

Figure 6.
[A] Setup diagram of the SLM platform for MCF applications. [B1, B2] photographs of the setup.

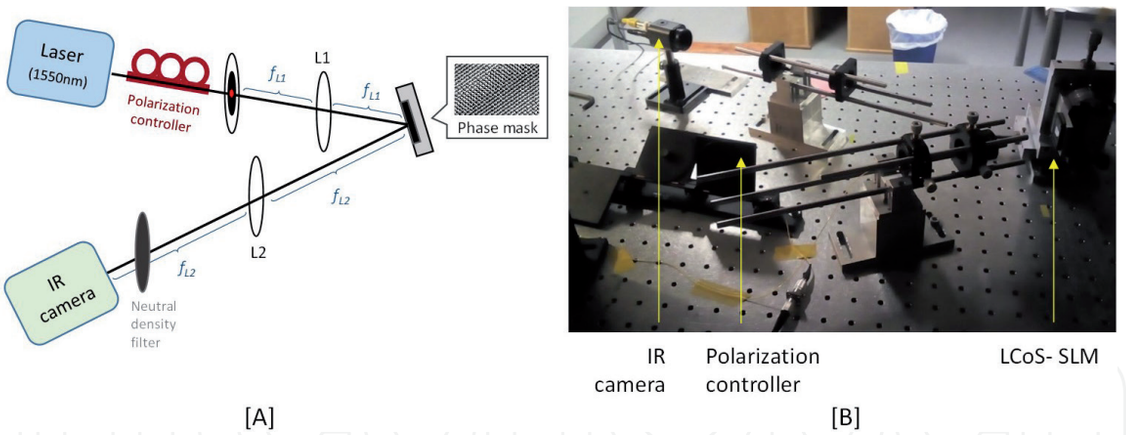

Figure 7.
[A] Hologram reconstruction scheme using an infrared (IR) laser of 1550 nm, a polarization controller, lens L1, an LCoS-SLM, lens L2, and an IR camera. [B] Photography of the presented setup.

The MCF contained four cores arranged in a quadrangular lattice pattern, with a side length of 36.25 μm and attenuation @1550 nm of 0.45 dB/km.

The nonreturn-to-zero (NRZ) signal was generated by a pattern generator (Agilent N4901B) using a pseudorandom binary sequence (PRBS) 2^{31}–1. This signal was injected to the tunable direct modulator laser to create 10 Gb/s optical signal. After the MCF, the signal was detected by avalanche photodiode (APD) receiver inside the small form-factor pluggable (SFP) transceiver.

3.2.2 CGH setup for PIC

In an effort to eliminate the phase distortion and enable the full Fourier transform scale by the focal length (*f*) factor, the optical system is designed based on the 4*f* system configuration. The implementation is the basis of a low distortion optical system.

The setup consists of devices such as two lenses (AC254–050-C-ML, AR coating 1050–1620 nm) L1 and L2 with a focal length of 75 and 250 mm, respectively; polarization controller; an infrared (IR) laser of 1550 nm (wavelength); a near-infrared (1460–1600 nm) camera (sensing area, 6.4 × 4.8 mm; resolution, 752 × 582; pixel size, 8.6 × 8.3 μm) for capturing the produced hologram; and a neutral density filter, to prevent saturation in the camera acquisition (see **Figure 7**) [8, 23].

4. Results and discussion

In this section, we present the experimental CGH results obtained for the SDM and PIC applications.

4.1 SLM platform for MCF

A BER of 1.2 × 10^{-3} was measured in the experiment described in Section 3.2.1. Test result shows an error-free transmission below the BER limit of 3.8 × 10^{-3} (7% hard-decision FEC) [54, 55] threshold.

Thus, the SLM framework was able to properly function as a spatial coupling interface between the SLM generated pattern and the MCF cores. The platform allows an easy adjustment of the generated phase mask (CGH), contributing to an effective dynamic optimization of the MCF fiber transmission [18].

Future work will be performed in order to optimize the current convergence, namely, improve the optical system components (e.g., lenses and collimator) and the implemented phase masks [18].

4.2 CGH for PIC applications

An integrated approach for compression applications implemented in an indium phosphide (InP) optical chip was fabricated to realize a Haar wavelet transform [53]. The HT is a wavelet-based method with promising attributes for compression transformation techniques. Their application in image processing and pattern recognition due to its simple design, fast computation power, and efficiency can be easily realized by optical planar interferometry [53, 56, 57].

The HT operations include low-pass (L) and high-pass (H) filters applied over one dimension at a time. This filtering operation corresponds to the calculation of the average between two neighbors' pixel values (LP) or the difference between them (HP) [57]. The HT is implemented with a two-level network composed by three asymmetric adiabatic couplers (AAC) 2 × 2, reproducing the required operations, i.e., the average (sum) and the difference (subtraction) between the optical input pair [53]. The 2D HT can be decomposed in four sub-bands, LL, LH, HL, and HH [57]. The LL gives the data compressed.

In the optical chip (or PIC), these four sub-bands can be extrapolated from the four output WG at the end of the three AAC network, as depicted in **Figure 8**.

The optical chip is composed of four distributed feedback (DFB) source lasers (L_1–L_4), three asymmetric adiabatic coupler (AAC_1–AAC_3), six positive-intrinsic-negative (PIN) photodiodes for network monitoring, six MMI splitters 1 × 2, one MMI splitter 2 × 2, and two spot size converters (SSC), at the correspondent HT network output LL (compression) and HH. Further details about the PIC can be found elsewhere [23, 53].

In the described SLM framework, the hologram is generated in an attempt to create the beam profile in the first order of diffraction when being displayed on the SLM. The CGH is expected to reproduce the four WG outputs of the PIC implementing the HT [23, 53] (see **Figure 8**).

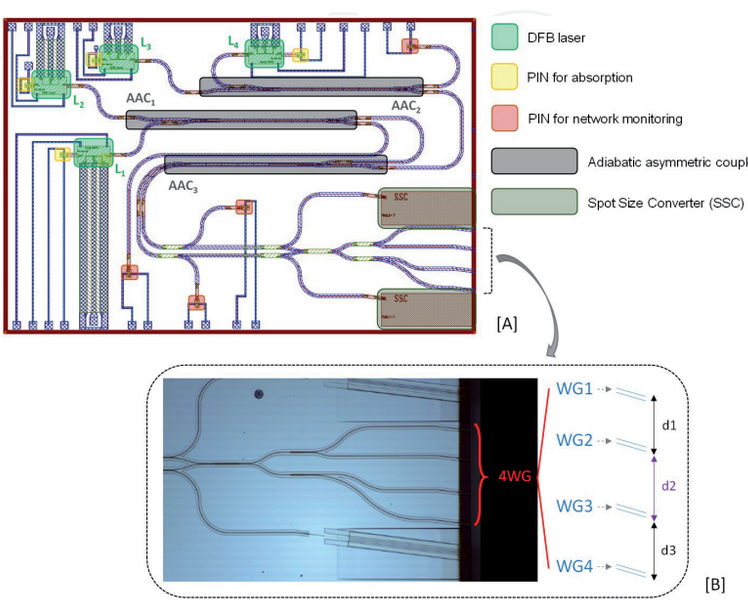

Figure 8.
[A] Design architecture of the PIC for data compression based on HT. [B] Measurements of the distance between the four WG at the end of the two-level compression network of the PIC [23].

In **Figure 9**, we present the obtained image from the hologram replay field generated with the initial (I_1) and optimized (I_{out}) CGH [8, 23].

The analysis of the obtained replay field images can be described by the steps described below:

i. Calculate the intensity integration of the image matrix, i.e., the sum of all elements along each line of the image matrix, depicted as S_{raw}.

ii. Application of the Savitzky–Golay (SG) filter to smoothen the intensity integration signal obtained in step (1), depicted as S_{SG}.

iii. Implementation of a first-order Gaussian fit curve to the filtered signal, depicted as *Gauss fit*.

iv. Extraction of Gaussian parameters to calculate the distances between the four beams (obtained from the CGH) and compare with the expected results (d_1, d_2, and d_3 from the optical chip).

Results from the integrated intensity profile of the replay field after the CGH optimization, i.e., after step (3), are presented in **Figure 10**.

The distance between the four beams was calculated from the center position of each beam profile, given by the Gaussian fit coefficient corresponding to the position of the center of the peak. The coefficients were obtained with 95% confidence bounds [23]. The deviation values (δ) between the generated holograms (i.e., initial I_1 and optimized I_{out}), when compared with the expected output of the optical chip (i.e., d_1, d_2 and d_3 from **Figure 8**), are presented in **Table 1** [23].

The measured power of the beams obtained by the integration intensity profiles is depicted in **Table 2** [23].

An improved hologram is achieved with the optimization of the linear phase mask CGH, i.e., with a reduction of up to 11% in the error factor (between

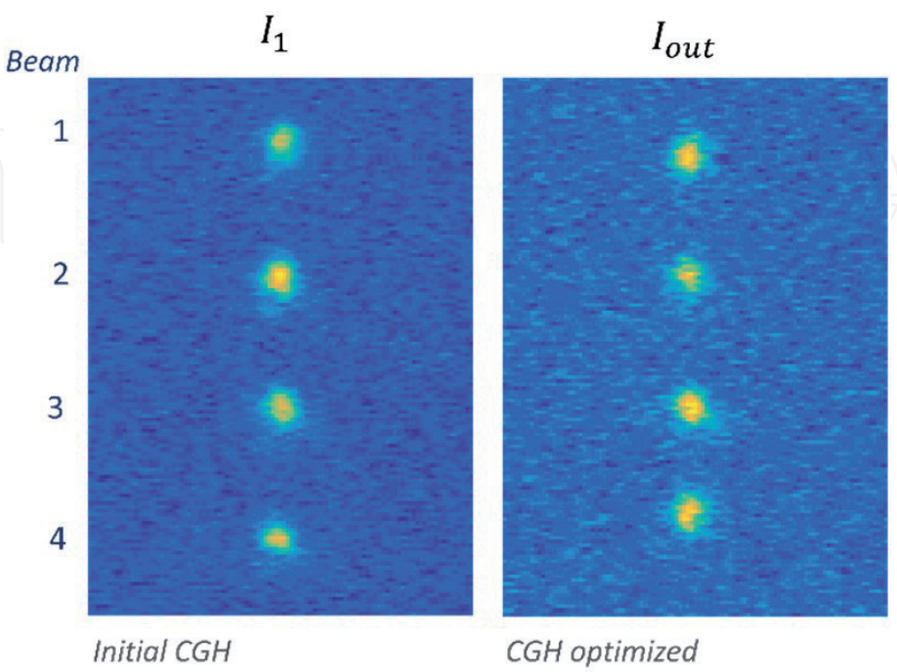

Figure 9.
Hologram replay field obtained by the IR camera with an (i) initial hologram (left figure) and (ii) optimized hologram (right figure).

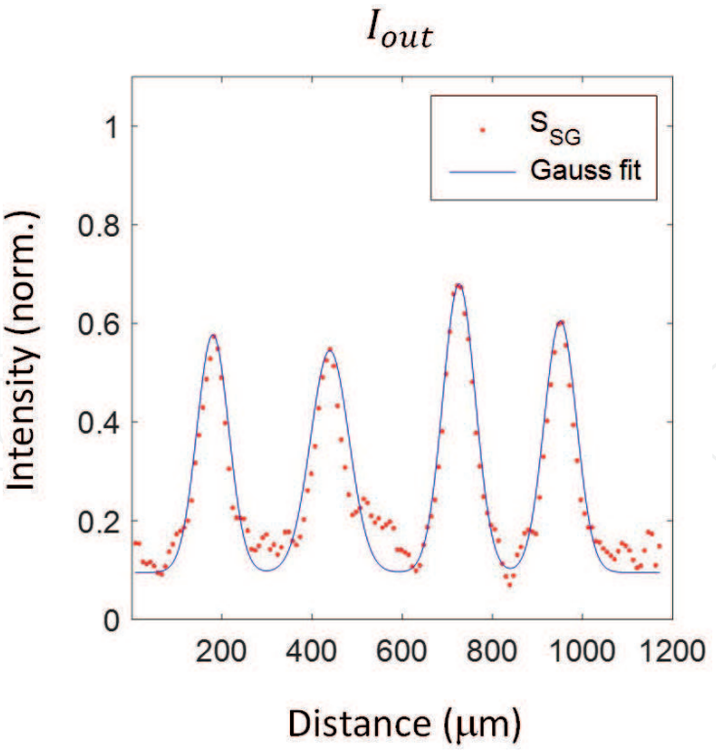

Figure 10.
Gaussian fit (Gauss fit, blue line) of smoothed integrated intensity signal from the replay field image (S_{SG}, red dots) of final optimized CGH [23].

	Initial CGH (%)	Optimized CGH (%)
δ_{d1}	19.76	7.48
δ_{d2}	1.96	2.90
δ_{d3}	14.31	9.44

Table 1.
Error factor (δ) values for d1, d2, and d3.

Beam	Initial CGH (u.a.)	Optimized CGH (u.a.)
1	6.30	5.12
2	8.21	5.78
3	7.18	6.37
4	7.69	5.51
Mean	7.35 ± 0.81	5.69 ± 0.52
Std (%)	11.17	9.14

Table 2.
Integration of the intensity profiles for the four beams.

initial and optimized holograms). Nonetheless, the loss of 1.1 dB identified on the mean beam power for the optimized CGH, an improved equalization between the beams was observed, with a 2% reduction in the standard deviation [23].

Algorithm improvements should be implemented to mitigate the power discrepancies between the four beams and optical artifacts associated with the diffraction of light, with the objective of mitigating the signal loss at the output of the optical chip.

A possible approach to correct some of this artifacts can be the application of the Gerchberg-Saxton [37] or simulated annealing [36] algorithms; nonetheless, due to the power loss (up to 9 dB [26]) associated with these approaches, they were not addressed in this implementation [23].

The phase mask that replicates the expected output of the PIC optical operation can be used to multiplex/demultiplex the obtained result. Furthermore, a phase mask, which addresses the HT operations, can also be applied to invert the compression induced by the HT (optically implemented in the PIC all-optical network with three AAC). Thus, a proof of concept of the PIC operation through the SLM coupling framework is expected [8, 23].

5. Conclusion

LCoS SLM technology implementation has been gaining importance in optical system applications, like telecom with the development of high-capacity optical components in system functionalities as switching (in ROADM), multiplexing and demultiplexing, and optical signal processing. In this chapter, a proof of concept on the implementation of a new SLM-based flexible coupling platform has been provided. We have also explored its implementation for applications in SDM systems and PIC characterization/testing. Furthermore, optimized methodologies to generate the CGH were developed and implemented. Main results include (i) BER = 1.2×10^{-3} for a SDM system, i.e., the use of the SLM to efficiently excite the different cores of a MCF, and (ii) CGH ($\delta \leq 1.5\%$) to feed/receive the output of an optical chip for data compression based on the HT. The demonstrations pave the way for the potential use of the SLM flexible platform in the development of multidimensional optical systems, by providing a versatile optical method which can overcome impairments introduced by the optical path in a MCF (e.g., by improving the setup alignment and excitation of different cores in MCF) and deliver a more robust optical methodology to assess and test photonic processors (e.g., offering a proof of concept of the PIC HT operation).

Acknowledgements

This work is funded by Fundação para a Ciência e a Tecnologia (FCT) through national funds under the scholarship PD/BD/105858/2014. It is also supported by FCT/MEC/MCTES and when applicable co-funded by FEDER – PT2020 partnership agreement under the project COMPRESS – PTDC/EEI-TEL/7163/2014 and the project UID/EEA/50008/2019. The authors acknowledge PICadvanced for its collaboration.

Author details

Cátia Pinho[1,2*], Isiaka Alimi[1,2], Mário Lima[1,2], Paulo Monteiro[1,2] and António Teixeira[1,2]

1 Instituto de Telecomunicações (IT), University of Aveiro, Aveiro, Portugal

2 Department of Electronics, Telecommunications and Informatics (DETI), University of Aveiro, Aveiro, Portugal

*Address all correspondence to: catiap@ua.pt

References

[1] He J et al. A survey on recent advances in optical communications. Computers and Electrical Engineering. 2014;**40**(1):216-240

[2] Ericsson. Ericsson Mobility Report. 2018

[3] Winzer PJ. Spatial multiplexing in fiber optics: The scaling of metro/core capacities. Bell Labs Technical Journal. 2014;**19**:22-30

[4] Ayyash M et al. Coexistence of WiFi and LiFi toward 5G: Concepts, opportunities, and challenges. IEEE Communications Magazine. 2016;**54**(2):64-71

[5] Pinho C, Shahpari A, Alimi I, Lima M, Teixeira A. Optical transforms and CGH for SDM systems. In: 18th International Conference on Transparent Optical Networks (ICTON 2016). 2016. pp. 1-4

[6] Alimi IA, Monteiro PP, Teixeira AL. Outage probability of multiuser mixed RF/FSO relay schemes for heterogeneous cloud radio access networks (H-CRANs). Wireless Personal Communications. 2017;**95**(1):27-41

[7] Alimi IA, Monteiro PP, Teixeira AL. Analysis of multiuser mixed RF/FSO relay networks for performance improvements in cloud computing-based radio access networks (CC-RANs). Optics Communication. 2017;**402**:653-661

[8] Pinho C et al. Flexible platform for feeding photonic integrated processors. In: The Thirteenth Advanced International Conference on Telecommunications (AICT 2017). 2017. pp. 1-4

[9] Grand View Research. Photonic Integrated Circuit (IC) Market Size Report. 2016

[10] Credence Research. Photonic Integrated Circuits Market. 2016

[11] Desurvire E et al. Science and technology challenges in XXIst century optical communications. Comptes Rendus Physique. 2011;**12**(4):387-416

[12] Ip E, Kahn JM. Increasing optical fiber transmission capacity beyond next-generation systems. In: LEOS 2008. 21st Annual Meeting of the IEEE Lasers and Electro-Optics Society 2008. pp. 606-607

[13] Shannon CE. A mathematical theory of communication. Bell System Technical Journal. 1948;**27**(3):379-423

[14] Alimi I, Shahpari A, Sousa A, Ferreira R, Monteiro P, Teixeira A. Challenges and opportunities of optical wireless communication technologies. In: Optical Communication Technology. London: IntechOpen; 2017. p. 41

[15] Richardson DJ, Fini JM, Nelson LE. Space-division multiplexing in optical fibres. Nature Photonics. 2013;**7**(5):354-362

[16] Yuan H, Furdek M, Muhammad A, Saljoghei A, Wosinska L, Zervas G. Space-division multiplexing in data center networks: On multi-Core fiber solutions and crosstalk-suppressed resource allocation. Journal of Optical Communications and Networking. 2018;**10**(4):272

[17] Morita I, Igarashi K, Tsuritani T. 1 Exabit/s·km transmission with multi-core fiber and spectral efficient modulation format. In: 2014 OptoElectronics and Communication Conference and Australian Conference on Optical Fibre Technology. 2014. pp. 316-318

[18] Pinho C et al. Spatial light modulator based flexible coupling platform for applications in SDM and PIC. In: 20th European Conference on Integrated Optics (ECIO 2018). 2018. pp. 238-240

[19] Richardson DJ. Unleashing the spatial domain in optical fiber communications. In: 2013 IEEE Photonics Society Summer Topical Meeting Series. 2013. pp. 70-71

[20] Essiambre R-J, Tkach RW. Capacity trends and limits of optical communication networks. Proceedings of the IEEE. 2012;**100**(5):1035-1055

[21] Carpenter J, Leon-Saval S, Eggleton BJ, Schröder J. Spatial light modulators for sub-systems and characterization in SDM. In: 2014 OptoElectronics and Communication Conference and Australian Conference on Optical Fibre Technology. 2014. pp. 23-24

[22] Lee HJ, Moon HS, Choi S-K, Park HS. Multi-core fiber interferometer using spatial light modulators for measurement of the inter-core group index differences. Optics Express. 2015;**23**(10):12555

[23] Pinho C et al. Flexible spatial light modulator based coupling platform for photonic integrated processors. International Journal on Advances in Telecommunications. 2018;**11**(1):20-31

[24] Smit M et al. An introduction to InP-based generic integration technology. Semiconductor Science and Technology—IOPscience. 2014;**29**(83001):1-41

[25] Goodman JW. Introduction to Fourier Optics. 2nd ed. Stanford: McGraw-Hill Companies; 1996

[26] Carpenter J. Holographic Mode Division Multiplexing in Optical Fibres. Cambridge, UK: University of Cambridge; 2012

[27] Lazarev G, Hermerschmidt A, Kr S. LCOS spatial light modulators: Trends and applications. In: Optical Imaging and Metrology: Advanced Technologies. Weinheim: Wiley-VCH. 2012. pp. 1-29

[28] Holoeye. "Spatial Light Modulators," Holoeye Photonics AG. 2013. [Online]. Available: http://holoeye.com/spatial-light-modulators/ [Accessed: 22-11-2017]

[29] Hamamatsu. Phase spatial light modulator LCOS-SLM. In: Opto-Semiconductor Handbook. Tokyo: Hamamatsu Photonics. 2012. pp. 1-14

[30] Kovachev M et al. Reconstruction of computer generated holograms by spatial light modulators. In: Multimedia Content Representation, Classification and Security. Vol. 4105. Berlin Heidelberg: Springer; 2006. pp. 706-713

[31] Younus SH, Hussein AT, Alresheedi MT, Elmirghani JMH. CGH for indoor visible light communication system. IEEE Access. 2017;**5**:24988-25004

[32] Torii Y, Balladares-Ocana L, Martinez-Castro J. An iterative Fourier transform algorithm for digital hologram generation using phase-only information and its implementation in a fixed-point digital signal processor. Optik (Stuttgart). 2013;**124**(22):5416-5421

[33] Ripoll O, Kettunen V, Herzig HP. Review of iterative Fourier-transform algorithms for beam shaping applications. Optical Engineering. 2004;**43**(11):2549-2556

[34] Pinho C, Lima M, Teixeira A. Optical compensation approach for SDM systems. In: XIII Symposium on Enabling Optical Networks and Sensors (SEONs 2016). 2016

[35] Lesem LB, Hirsch PM, Jordan JA. The Kinoform: A new wavefront reconstruction device. IBM Journal of Research and Development. 1969;**13**(2):150-155

[36] Carpenter J, Wilkinson TD. Graphics processing unit–accelerated holography by simulated annealing. Optical Engineering. 2010;**49**(9):095801-095807

[37] Gerchberg R, Saxton WO, Gerchberg BRW, Saxton WO. A practical algorithm for the determination of phase from image and diffraction plane pictures. Optik (Stuttgart). 1972;**35**(2):237-246

[38] Collings N, Davey T, Christmas J, Chu D, Crossland B. The applications and technology of phase-only liquid crystal on silicon devices. Journal of Display Technology. 2011;**7**(3):112-119

[39] Roelens MAF et al. Dispersion trimming in a reconfigurable wavelength selective switch. Journal of Lightwave Technology. 2008;**26**(1):73-78

[40] Wang M et al. LCoS SLM study and its application in wavelength selective switch. Photonics. 2017;**4**(2):22

[41] Turunen J, Wyrowski F. Diffractive Optics for Industrial and Commercial Applications. Berlin: John Wiley & Sons; 1997

[42] Osten W, Kohler C, Liesener J. Evaluation and application of spatial light modulators for optical metrology. In: Óptica Pura y Applicada, Reunión Española de Optoelectrónica, OPTOEL'05. 2005. pp. 71-81

[43] Varga JJM et al. Preparing arbitrary pure states of spatial qudits with a single phase-only spatial light modulator. Journal of Physics Conference Series. Apr. 2015;**605**(1):012035-012036

[44] Schroder J, Roelens MAF, Du LB, Lowery AJ, Eggleton BJ. LCOS based waveshaper technology for optical signal processing and performance monitoring. In: 17th Opto-Electronics and Communications Conference, 2012. 2012. pp. 859-860

[45] Keyworth BP. ROADM subsystems and technologies. In: OFC/NFOEC Technical Digest. Optical Fiber Communication Conference, 2005. Vol. 3. 2005. p. 4

[46] de Hennin S, Wall P, Moffat SH, Keyworth BP, Colbourne PD. Addressing manufacturability and reliability of MEMS-based WSS. In: OFC/NFOEC 2007—Conference on Optical Fiber Communication and the National Fiber Optic Engineers Conference; 2007; pp. OWV1-3

[47] Strasser TA, Wagener JL. Wavelength-selective switches for ROADM applications. IEEE Journal of Selected Topics in Quantum Electronics. 2010;**16**(5):1150-1157

[48] Shiraiwa M, Furukawa H, Miyazawa T, Awaji Y, Wada N. High-speed wavelength resource reconfiguration system concurrently establishing/removing multiwavelength signals. IEEE Photonics Journal. 2016;**8**(2):1-7

[49] Lhermite J, Suran E, Kermene V, Louradour F, Desfarges-Berthelemot A, Barthélémy A. Coherent combining of 49 laser beams from a multiple core optical fiber by a spatial light modulator. Optics Express. 2010;**18**(5):4783-4789

[50] Slinger C, Cameron C, Stanley M. Computer-generated holography as a generic display technology. IEEE Computer Society. 2005;**38**(8):46-53

[51] Tricoles G. Computer generated holograms: An historical review. Applied Optics. 1987;**26**(20):4351

[52] MathWorks. R2018b—MATLAB and Simulink Product Families. The MathWorks, Inc. [Online]. Available: https://www.mathworks.com/products/new_products/latest_features.html [Accessed: 13-04-2019]

[53] Pinho C, Neto B, Morgado TM, Neto H, Lima M, Teixeira A. InP AAC for Data Compression Applications. IET Optoelectronics. 2019;**13**(2):67-71

[54] Chang F, Onohara K, Mizuochi T. Forward error correction for 100 G transport networks. IEEE Communications Magazine. 2010;**48**(3):S48-S55

[55] Matiss A et al. Performance of an integrated coherent receiver module for up to 160G DP-QPSK transmission systems. Journal of Lightwave Technology. 2011;**29**(7):1026-1032

[56] Ashok V, Balakumaran T, Gowrishankar C, Vennila ILA, Kumar AN. The fast Haar wavelet transform for signal & image processing. International Journal of Computer Science and Information Security. 2010;**7**(1):126-130

[57] Parca G, Teixeira P, Teixeira A. All-optical image processing and compression based on Haar wavelet transform. Applied Optics. 2013;**52**(12):2932-2939